

## Chapter 1

# A Mathematical Theory of Climate Sensitivity or, How to Deal With Both Anthropogenic Forcing and Natural Variability?

Michael Ghil

*Ecole Normale Supérieure, 75005 Paris, FRANCE, and  
University of California, Los Angeles, CA 90095, USA  
ghil@lmd.ens.fr\**

Recent estimates of climate evolution over the coming century still differ by several degrees. This uncertainty motivates the work presented here. There are two basic approaches to apprehend the complexity of climate change: deterministically nonlinear and stochastically linear, i.e. the Lorenz and the Hasselmann approach. The grand unification of these two approaches relies on the theory of random dynamical systems. We apply this theory to study the random attractors of nonlinear, stochastically perturbed climate models. Doing so allows one to examine the interaction of internal climate variability with the forcing, whether natural or anthropogenic, and to take into account the climate system's non-equilibrium behavior in determining climate sensitivity.

This non-equilibrium behavior is due to a combination of nonlinear and random effects. We give here a unified treatment of such effects from the point of view of the theory of dynamical systems and of their bifurcations. Energy balance models are used to illustrate multiple equilibria, while multi-decadal oscillations in the thermohaline circulation illustrate the transition from steady states to periodic behavior. Random effects are introduced in the setting of random dynamical systems, which permit a unified treatment of both nonlinearity and stochasticity. The combined treatment of nonlinear and random effects is applied to a stochastically perturbed version of the classical Lorenz convection model.

Climate sensitivity is then defined mathematically as the derivative of an appropriate functional or other function of the system's state with respect to the bifurcation parameter. This definition is illustrated by using numerical results for a model of the El Niño–Southern Oscillation. The concept of a hierarchy of models is the thread that runs across this chapter, and the robustness of elementary bifurcations across such a hierarchy is emphasized.

### 1.1. Introduction

The global climate system is composed of a number of subsystems — atmosphere, biosphere, cryosphere, hydrosphere and lithosphere — each of which has distinct characteristic times, from days and weeks to centuries and millennia. Each subsystem, moreover, has its own internal variability, all other things being constant, over a fairly broad range of time scales. These ranges overlap between one subsystem and another. The interactions between the subsystems thus

\*additional E-address: ghil@atmos.ucla.edu.

give rise to climate variability on all time scales. We outline here the rudiments of the way in which *dynamical systems theory* provides an understanding of this vast range of variability. Such an understanding proceeds through the study of successively more complex patterns of behavior. These spatio-temporal patterns are studied within narrower ranges of time scales, such as intraseasonal, interannual, interdecadal and multi-millennial. The main results of dynamical systems theory that have demonstrated

their importance for the study of climate variability involve *bifurcation theory* and the *ergodic theory* of dynamical systems. More recently, the theory of random dynamical systems has made substantial contributions as well.

Before proceeding with the outline of this chapter, we point out that the successive reports of the Intergovernmental Panel on Climate Change [IPCC: Houghton *et al.* (1991); Solomon *et al.* (2007)] have mainly considered the contributions of uncertainty in the representation of various physical processes to the uncertainty in the climate's equilibrium sensitivity, as defined in Sec. 1.5.1 below. The well-known result of the IPCC reviews of numerous studies in this direction is that cloud feedbacks are the most important contributor to said uncertainty.

General circulation models (GCMs), on which the IPCC reports rely more and more, do not have a sufficient degree of internal variability — largely but not exclusively due to their still relatively low numerical resolution [e.g., ?]. Thus it is cloud feedbacks, and their paramount effect on equilibrium sensitivity, that seem to dominate the IPCC estimates of future climate change as well.

The main purpose of this chapter is to illustrate the way in which natural climate variability could affect these estimates. We do not attempt, at this time, to provide a quantitative evaluation of the extent to which this variability's effect would modify IPCC conclusions, whether they relate to cloud feedbacks or to other types of feedbacks. Among the latter, the oceanic circulation also plays an important role.

In the next section, we describe the climate systems dominant balance between incoming solar radiation, dominated by short waves, and outgoing terrestrial radiation, dominated by long waves. This balance is consistent with the existence of multiple equilibria of surface temperatures.

Such *multiple equilibria* are also present for other balances of climatic actions and reactions. Thus, on the intraseasonal time scale, the ther-

mal driving of the mid-latitude westerly winds is countered by surface friction and mountain drag. Multiple equilibria typically arise from saddle-node bifurcations of the governing equations. Transitions from one equilibrium to another may result from small and random pushes — a typical case of minute causes having large effects in the long term.

In Sec. 1.3, we sketch the oceans' overturning circulation between cold regions, where water is heavier and sinks, and warm regions, where it is lighter and rises. The effect of temperature on the water masses density and, hence, motion is in competition with the effect of salinity: density increases, through evaporation and brine formation, compete further with decreases in salinity and, hence, density through precipitation and river run-off. These competing effects can also give rise to two distinct equilibria.

In the present-day oceans, a *thermohaline* circulation prevails, in which the temperature effects dominate. In the remote past, about 50 Myr ago, a *halothermal* circulation may have obtained, with salinity effects dominating. In a simplified mathematical setting, these two equilibria arise by a pitchfork bifurcation that breaks the problems mirror symmetry. On shorter time scales, of decades-to-millennia, oscillations of intensity and spatial pattern in the thermohaline circulation seem to be the dominant mode of variability. We show how interdecadal oscillations in the oceans' circulation arise by Hopf bifurcation.

In Sec. 1.4, we address the way that faster processes, modeled as random effects, can interact with the slower, nonlinear ones. The combined treatment of the nonlinear and stochastic processes can reveal amazingly fine structure in the climate systems behavior, but also — and rather surprisingly — add robustness and predictability to the results.

In Sec. 1.5, we discuss the way that climate sensitivity can be defined in the stochastic vs. the deterministic context. Concluding remarks follow in Sec. 1.6.

## 1.2. Energy-Balance Models and the Modeling Hierarchy

The concepts and methods of the theory of deterministic dynamical systems (Andronov and Pontryagin, 1937; Arnol'd, 1983; Guckenheimer and Holmes, 1983) have been applied first to simple models of atmospheric and oceanic flows, starting about fifty years ago (Lorenz, 1963; Stommel, 1961). More powerful computers now allow their application to fairly realistic and detailed models of the atmosphere, ocean, and the coupled atmosphere–ocean system. We start therefore by presenting such a hierarchy of models.

This presentation is interwoven with that of the successive bifurcations that lead from simple to more complex solution behavior for each climate model. Useful tools for comparing model behavior across the hierarchy and with observations are provided by ergodic theory (Eckmann and Ruelle, 1985; Ghil *et al.*, 2008a). Among these, advanced methods for the analysis and prediction of uni- and multivariate time series play an important role.

### 1.2.1. Radiation balance and energy-balance models (EBMs)

The concept of a modeling hierarchy in climate dynamics was introduced by Schneider and Dickinson (1974); it is discussed in greater detail by Ghil and Robertson (2000) and by Dijkstra and Ghil (2005). At present, the best-developed hierarchy is for atmospheric models. These models were originally developed for weather simulation and prediction on the time scale of hours to days. Currently they serve in a stand-alone mode or coupled to oceanic and other models to address climate variability on all time scales.

The first rung of the modeling hierarchy for the atmosphere is formed by zero-dimensional (0-D) models, where the number of dimensions, from zero to three, refers to the number of independent space variables used to describe the model domain, i.e. to physical-space dimensions.

Such 0-D models essentially attempt to follow the evolution of global surface-air temperature as a result of changes in global radiative balance:

$$c \frac{d\bar{T}}{dt} = R_i - R_o, \quad (1.1a)$$

$$R_i = \mu Q_0 \{1 - \alpha(\bar{T})\}, \quad (1.1b)$$

$$R_o = \sigma m(\bar{T})(\bar{T})^4. \quad (1.1c)$$

Here  $R_i$  and  $R_o$  are incoming solar radiation and outgoing terrestrial radiation. The heat capacity  $c$  is that of the global atmosphere, plus that of the global ocean or some fraction thereof, depending on the time scale of interest: one might only include in  $c$  the ocean mixed layer when interested in subannual time scales but the entire ocean when studying paleoclimate.

The rate of change of  $\bar{T}$  with time  $t$  is given by  $d\bar{T}/dt$ , while  $Q_0$  is the solar radiation received at the top of the atmosphere,  $\sigma$  is the Stefan-Boltzmann constant, and  $m$  is an insolation parameter, equal to unity for present-day conditions. To have a closed, self-consistent model, the planetary reflectivity or albedo  $\alpha$  and grayness factor  $m$  have to be expressed as functions of  $\bar{T}$ ;  $m = 1$  for a perfectly black body and  $0 < m < 1$  for a grey body like planet Earth.

There are two kinds of one-dimensional (1-D) atmospheric models, for which the single spatial variable is latitude or height, respectively. The former are so-called energy-balance models (EBMs), which consider the generalization of the model (2.1) for the evolution of surface-air temperature  $T = T(x, t)$ , say,

$$c(x) \frac{\partial \bar{T}}{\partial t} = R_i - R_o + D. \quad (1.2)$$

Here the terms on the right-hand side can be functions of the meridional coordinate  $x$  (latitude, co-latitude, or sine of latitude), as well as of time  $t$  and temperature  $T$ . The horizontal heat-flux term  $D$  expresses heat exchange between latitude belts; it typically contains first and second partial derivatives of  $T$  with respect to  $x$ . Hence the rate of change of local temperature  $T$  with respect to time also becomes a partial derivative,  $\partial \bar{T} / \partial t$ . Such models were intro-

duced independently by Budyko (1969) and by Sellers (1969).

The first striking results of theoretical climate dynamics were obtained in showing that Eq. (1.2) could have two stable steady-state solutions, depending on the value of the insolation parameter  $\mu$ , cf. Eq. (1.1b). This multiplicity of stable steady states, or physically possible climates of our planet, can be explained, in its simplest form, in the 0-D model given by Eq. (1.1).

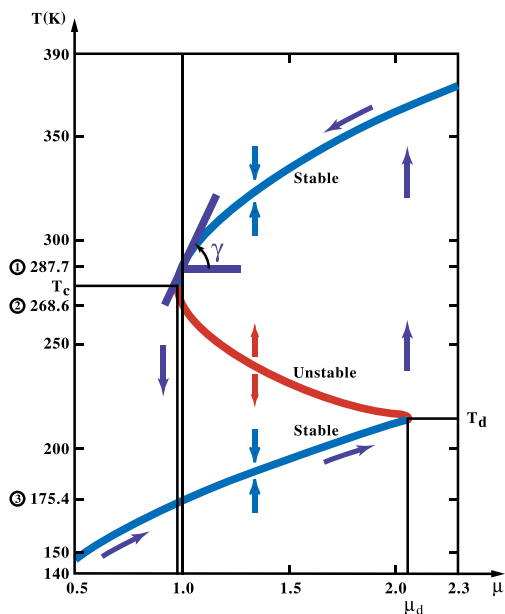


Fig. 1.1. Bifurcation diagram for the solutions of an energy-balance model (EBM), showing the global-mean temperature  $\bar{T}$  vs. the fractional change  $\mu$  of insolation at the top of the atmosphere. The arrows pointing up and down at about  $\mu = 1.4$  indicate the stability of the branches: towards a given branch if it is stable and away if it is unstable. The other arrows show the hysteresis cycle that global temperatures would have to undergo for transition from the upper stable branch to the lower one and back. The angle  $\gamma$  gives the measure of the present climates sensitivity to changes in insolation. [After Ghil and Childress (1987) with permission from Springer-Verlag.]

The physical explanation resides in the fact that — for a fairly broad range of  $\mu$ -values around  $\mu = 1.0$  — the curves for  $R_i$  and  $R_o$  as a function of  $\bar{T}$  intersect in 3 points. One of these

points corresponds to the present climate (highest  $\bar{T}$ -value), and another one to an ice-covered planet (lowest  $\bar{T}$ -value); both of these are stable, while the third one (intermediate  $\bar{T}$ -value) is unstable. To obtain this result, it suffices to make two assumptions: (i) that  $\alpha = \alpha(\bar{T})$  is a piecewise-linear function of  $\bar{T}$ , with high albedo at low temperature, due to the presence of snow and ice, and low albedo at high  $\bar{T}$ , due to their absence; and (ii) that  $m = m(\bar{T})$  is a smooth, increasing function of  $\bar{T}$  that attempts to capture in its simplest form the greenhouse effect of trace gases and water vapor.

The bifurcation diagram of a 1-D EBM, like the one of Eq. (1.2), is shown in Fig. 1.1. It displays the model's mean temperature  $\bar{T}$  as a function of the fractional change  $\mu$  in the insolation  $Q = Q(x)$  at the top of the atmosphere. The S-shaped curve in the figure arises from two back-to-back *saddle-node bifurcations*.

The normal form of the first one is

$$\dot{X} = \mu - X^2. \tag{1.3}$$

Here  $X$  stands for a suitably normalized form of  $\bar{T}$  and  $\dot{X}$  is the rate of change of  $X$ , while  $\mu$  is a parameter that measures the stress on the system, in particular a normalized form of the insolation parameter.

The uppermost branch corresponds to the steady-state solution  $X = +\mu^{1/2}$  of Eq. (1.3) and it is stable. This branch matches rather well Earth's present-day climate for  $\mu = 1.0$ ; more precisely the steady-state solution  $T = T(x; \mu)$  of the full 1-D EBM (not shown) matches closely the annual mean temperature profile from instrumental data over the last century.

The intermediate branch starts out at the left as the second solution,  $X = -\mu^{1/2}$ , of Eq. (1.3) and it is unstable. It blends smoothly into the upper branch of a coordinate-shifted and mirror-reflected version of Eq. (1.3), say

$$\dot{X} = \mu - X^2. \tag{1.4}$$

This branch,  $X = X_0 + (\mu_0 - \mu)^{1/2}$ , is also unstable. Finally, the lowermost branch in Fig. 1.1

is the second steady-state solution of Eq. (1.4),  $X = X_0(\mu_0 - \mu)^{1/2}$ , and it is stable, like the uppermost branch. The lowermost branch corresponds to an ice-covered planet at the same distance from the Sun as Earth.

The fact that the upper-left bifurcation point  $(\mu_c, T_c)$  in Fig. 1.1 is so close to present-day insolation values created great concern in the climate dynamics community in the mid-1970s, when these results were obtained. Indeed, much more detailed computations (see below) confirmed that a reduction of about 2–5% of insolation values would suffice to precipitate Earth into a deep freeze. The great distance of the lower-right bifurcation point  $(\mu_d, T_d)$  from present-day insolation values, on the other hand, suggests that one would have to nearly double atmospheric opacity, say, for the Earth's climate to jump back to more comfortable temperatures.

The results here follow Ghil (1976). Held and Suarez (1974) and North (1975) obtained similar results, and a detailed comparison between EBMs appears in Chapter 10 of Ghil and Childress (1987). The robustness of a saddle-node bifurcation has been documented by Wetherald and Manabe (1975, their Fig. 5 and associated text) in a slightly simplified GCM, coupled to a swamp ocean. Likewise, North *et al.* (1983) have found the manifestation of a hysteresis cycle among such bifurcations — their “small-ice-cap instability” — in a two-dimensional (2-D) EBM resolving the continents and seasons. Please see the next subsection for the rung occupied by each of these two models in the climate modeling hierarchy.

### 1.2.2. *Other atmospheric processes and models*

The 1-D atmospheric models in which the details of radiative equilibrium are investigated with respect to a height coordinate  $z$  (geometric height, pressure, etc.) are often called *radiative-convective models* (Ramanathan and Coakley, 1978). This name emphasizes the key

role that convection plays in vertical heat transfer. While these models preceded historically EBMs as rungs on the modeling hierarchy, it was only recently shown that they, too, could exhibit multiple equilibria (Li *et al.*, 1997). The word (stable) equilibrium, here and in the rest of this article, refers simply to a (stable) steady state of the model, rather than a true thermodynamic equilibrium.

2-D atmospheric models are also of two kinds, according to the third space coordinate that is not explicitly included. Models that resolve explicitly two horizontal coordinates, on the sphere or on a plane tangent to it, tend to emphasize the study of the dynamics of large-scale atmospheric motions. They often have a single layer or two. Those that resolve explicitly a meridional coordinate and height are essentially combinations of EBMs and radiative-convective models and emphasize therewith the thermodynamic state of the system, rather than its dynamics.

Yet another class of horizontal 2-D models is the extension of EBMs to resolve zonal, as well as meridional surface features, in particular land-sea contrasts (North *et al.*, 1983). We shall see in Sec. 1.3.2 how such a 2-D EBM is used, when coupled to an oceanic model.

Schneider and Dickinson (1974) and Ghil and Robertson (2000) discuss additional types of 1-D and 2-D atmospheric models and give references to these and to the types discussed above, along with some of their main applications. Finally, to encompass and resolve the main atmospheric phenomena with respect to all three spatial coordinates, GCMs occupy the pinnacle of the modeling hierarchy.

The dependence of mean zonal temperature on the insolation parameter  $\mu$  (the normalized “solar constant”) — as obtained for 1-D EBMs and shown in Fig. 1.1 here — was confirmed, to the extent possible, by using a simplified GCM, coupled to a swamp ocean model. More precisely, forward integrations with a GCM cannot confirm the presence of the intermediate, unsta-

ble branch. Nor was it possible in the mid-70s, when this numerical experiment was done, to reach the deep-freeze stable branch, because of the GCMs computational limitations. But the parabolic shape of the upper, present-daylike branch near the upper-left bifurcation point in our figure, cf. Eq. (1.3), was well supported by the GCM simulations.

Ghil and Robertson (2000) also describe the separate hierarchies that have grown over the last quarter-century in modeling the ocean and the coupled ocean-atmosphere system. More recently, an overarching hierarchy of earth-system models that encompass all the subsystems of interest, atmosphere, biosphere, cryosphere, hydrosphere and lithosphere has been developing. Eventually, the partial results about each subsystem's variability, outlined in this section and the next one, will have to be verified from one rung to the next of the Earth-system modeling hierarchy.

In the meantime, we have described in the present section here the robustness of bifurcation results for the multiple equilibria associated with the Earth system's energy balance, from 0-D EBMs all the way to full, 3-D GCMs. In the next section, we discuss the robustness of bifurcation results on both multiple equilibria and oscillations, across a modeling hierarchy for the ocean's circulation.

### 1.3. Oscillations in the Oceans' Thermohaline Circulation

#### 1.3.1. Theory and simple models

Historically, the thermohaline circulation (THC) was first among the climate systems major processes to be studied using a very simple mathematical model. Stommel (1961) formulated a two-box model and showed that it possessed multiple equilibria.

A sketch of the Atlantic Oceans THC and its interactions with the atmosphere and cryosphere on long time scales is shown in Fig. 1.2. These interactions can lead to climate

oscillations with multi-millennial periods, such as the Heinrich events, and are summarized in the figure's caption. An equally schematic view of the global THC is provided by the widely known "conveyor belt" diagram. The latter diagram captures greater horizontal, 2-D detail but it does not commonly include the THC's interactions with water in both its gaseous and solid phases, which our Fig. 1.2 here does include.

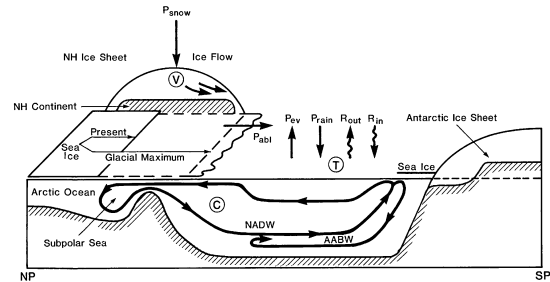


Fig. 1.2. Diagram of an Atlantic meridional cross section from North Pole (NP) to South Pole (SP), showing mechanisms likely to affect the thermohaline circulation (THC) on various time-scales. Changes in the radiation balance  $R_{in} - R_{out}$  are due, at least in part, to changes in extent of Northern Hemisphere (NH) snow and ice cover  $V$ , and to how these changes affect the global temperature  $T$ ; the extent of Southern Hemisphere ice is assumed constant, to a first approximation. The change in hydrologic cycle expressed in the terms  $P_{rain} - P_{evap}$  for the ocean and  $P_{snow} - P_{abl}$  for the snow and ice is due to changes in ocean temperature. Deep-water formation in the North Atlantic Subpolar Sea (North Atlantic Deep Water: NADW) is affected by changes in ice volume and extent, and regulates the intensity  $C$  of the THC; changes in Antarctic Bottom Water (AABW) formation are neglected in this approximation. The THC intensity  $C$  in turn affects the systems temperature, and is also affected by it. [After Ghil *et al.* (1987) with permission from Springer-Verlag.]

Basically, the THC is due to denser water sinking, lighter water rising, and water-mass continuity closing the circuit through near-horizontal flow between the areas of rising and sinking. The effects of temperature and salinity on the ocean waters density,  $\rho = \rho(T, S)$ , oppose each other: the density  $\rho$  decreases as  $T$  increases and it increases as  $S$  increases. It is these two effects that give the thermohaline circulation its name, from the Greek words for  $T$

and  $S$ . In high latitudes,  $\rho$  increases as the water loses heat to the air above and, if sea ice is formed, as the water underneath is enriched in brine. In low latitudes,  $\rho$  increases due to evaporation but decreases due to sensible heat flux into the ocean.

For the present climate, the temperature effect is stronger than the salinity effect, and ocean water is observed to sink in certain areas of the high-latitude North Atlantic and Southern Ocean — with very few and limited areas of deep-water formation elsewhere — and to rise everywhere else. Thus, in a *thermohaline* regime,  $T$  is more important than  $S$  and hence comes before it.

During some remote geological times, deep water may have formed in the global ocean near the equator; such an overturning circulation of opposite sign to that prevailing today has been dubbed *halothermal*,  $S$  before  $T$ . The quantification of the relative effects of  $T$  and  $S$  on the oceanic water masses buoyancy in high and low latitudes is far from complete, especially for paleocirculations; the association of the latter with salinity effects that exceed the thermal ones (Kennett and Stott, 1991) is thus rather tentative.

To study the reversal of the abyssal circulation, due to the opposite effects of  $T$  and  $S$ , Stommel considered a two-box model, with two pipes connecting the two boxes. He showed that the system of two nonlinear, coupled ordinary differential equations that govern the temperature and salinity differences between the two well-mixed boxes has two stable steady-state solutions; these two steady states are distinguished by the direction of flow in the upper and lower pipe.

Stommel's paper was primarily concerned with distinct local convection regimes, and hence vertical stratifications, in the North Atlantic and the Mediterranean or the Red Sea, say. Today, we mainly think of one box as representing the low latitudes and the other one the high latitudes in the global THC (Marotzke,

2000; Dijkstra and Ghil, 2005).

The next step in the hierarchical modeling of the THC is that of 2-D meridional plane models, in which the temperature and salinity fields are governed by coupled nonlinear partial differential equations with two independent space variables, latitude and depth, say. Given boundary conditions for such a model that are symmetric about the Equator, as the equations themselves are, one expects a symmetric solution, in which water either sinks near the poles and rises everywhere else (thermohaline) or sinks near the Equator and rises everywhere else (halothermal). These two symmetric solutions would correspond to the two equilibria of Stommel's box model of 1961.

In fact, *symmetry breaking* can occur, leading gradually from a symmetric two-cell circulation to an antisymmetric one-cell circulation. In between, all degrees of dominance of one cell over the other are possible. A situation lying somewhere between the two seems to resemble most closely the meridional overturning diagram of the Atlantic Ocean in Fig. 1.2.

This symmetry breaking can be described by a *pitchfork bifurcation*:

$$\dot{X} = \mu - X^3. \quad (1.5)$$

Here  $X$  stands for the amount of asymmetry in the solution, so that  $X = 0$  is the symmetric branch, and  $\mu$  is a parameter that measures the stress on the system, in particular a normalized form of the buoyancy flux at the surface. For  $\mu < 0$  the symmetric branch is stable, while for  $\mu > 0$  the two branches  $X = \pm\mu^{1/2}$  inherit its stability.

In the 2-D THC problem, the left cell dominates on one branch, while the right cell dominates on the other: for a given value of  $\mu$ , the two stable steady-state solutions — on the  $\{X = +\mu^{1/2}\}$  branch and on the  $\{X = -\mu^{1/2}\}$  branch — are mirror images of each other. The idealized THC in Fig. 1.2, with the North Atlantic Deep Water extending to the Southern Oceans polar front, corresponds to one of these two branches.

In theory, therefore, a mirror-image circulation, with the Antarctic Bottom Water extending to the North Atlantic's polar front, is equally possible.

### 1.3.2. Bifurcation diagrams for GCMs

Bryan (1986) was the first to document transition from a two-cell to a one-cell circulation in a simplified ocean GCM with idealized, symmetric forcing. Results of coupled ocean-atmosphere GCMs, however, have led to questions about the realism of more than one stable THC equilibrium. The situation with respect to the THC's pitchfork bifurcation (1.5) is thus subtler than it was with respect to Fig. 1.1 for radiative equilibrium.

In the previous section, atmospheric GCMs — both 2-D (North *et al.*, 1983) and 3-D (Wetherald and Manabe, 1975) — confirmed essentially the EBM results. The results obtained in climbing the rungs of the modeling hierarchy for the THC appear, however, to be still in need of further clarification.

To facilitate this clarification, Dijkstra (2007) defined an integral indicator  $\Sigma$  associated with the multiple-equilibria regime of the Atlantic Ocean's THC,

$$\Sigma = M_{\text{ov}}(\theta_N) - M_{\text{ov}}(\theta_S). \quad (1.6)$$

In the above definition, the sign of  $M_{\text{ov}}(\theta)$ , positive or negative, states whether the Atlantic exports salt or fresh water across a particular parallel  $\theta$ ; here  $\theta_N$  passes through the southern tip of Greenland, and  $\theta_S$  passes through the southern tip of Africa. The present notation differs slightly from the original one, for clarity of presentation. When  $\Sigma > 0$ , the Atlantic's THC is in the multiple-equilibria regime, i.e. a thermohaline and a halothermal circulation can coexist.

Recent observational studies (Bryden *et al.*, 2011) and ocean reanalyses (Hawkins *et al.*, 2011) confirm that the Atlantic Ocean's THC is actually in this regime at the present time. On the other hand, the ocean GCMs used in the third Coupled-Model Intercomparison Pro-

gram (CMIP3) — on which the conclusions of the IPCC's Fourth Assessment Report (Solomon *et al.*, 2007) were based — tended to have a systematic bias in their evaporation-minus-precipitation fluxes (Drijfhout *et al.*, 2011), which led to the wrong sign of  $\Sigma$  in these models.

Thus a failure of high-end models in the hierarchy to confirm results obtained at the hierarchy's lower end does not necessarily imply it's the simpler models that are wrong. To the contrary, such a failure might well indicate that the high-end models, no matter how detailed, can still be quite wrong.

Internal variability of the THC with smaller and more regular excursions than the huge and totally irregular jumps associated with bistability was studied intensively in the late 1980s and the 1990s. These studies placed themselves on various rungs of the modeling hierarchy, from box models through 2-D models and all the way to ocean GCMs. A summary of the different kinds of oscillatory variability found in the latter appears in Table 1.1. Such oscillatory behavior seems to match more closely the instrumentally recorded THC variability, as well as the paleoclimatic records for the recent geological past, than bistability.

The (multi)millennial oscillations interact with variability in the surface features and processes shown in Fig. 1.2. Chen and Ghil (1996), in particular, studied some of the interactions between atmospheric processes and the THC. They used a so-called hybrid coupled model, namely a (horizontally) 2-D EBM, coupled to a rectangular-box version of the North Atlantic rendered by a low-resolution ocean GCM. This hybrid models regime diagram is shown in Fig. 1.3(a). A steady state is stable for high values of the coupling parameter or of the EBMs diffusion parameter  $d$ . Interdecadal oscillations with a period of 40–50 years are self-sustained and stable for low values of these parameters.

The self-sustained THC oscillations in question are characterized by a pair of vortices of opposite sign that grow and decay in quadra-

Table 1.1. Oscillations in the oceans' thermohaline circulation.

| Time scale | Phenomena  | Mechanism <sup>a</sup>  |
|------------|--|---|
| Decadal    | <ul style="list-style-type: none"> <li>· Local migration of surface anomalies in the northwest corner of the ocean basin</li> <li>· Gyre advection in mid-latitudes</li> </ul> | <ul style="list-style-type: none"> <li>· Localized surface density anomalies due to surface coupling</li> <li>· Gyre advection</li> </ul> |
| Centennial | Loop-type, meridional circulation  | Conveyor-belt advection of density anomalies  |
| Millennial | Relaxation oscillation, with "flushes" and superimposed decadal fluctuations   | Bottom water warming, due to strong braking effect of salinity forcing  |

<sup>a</sup> Complete references to these mechanisms are given in Ghil (1994); they include both simplified and full ocean GCMs.

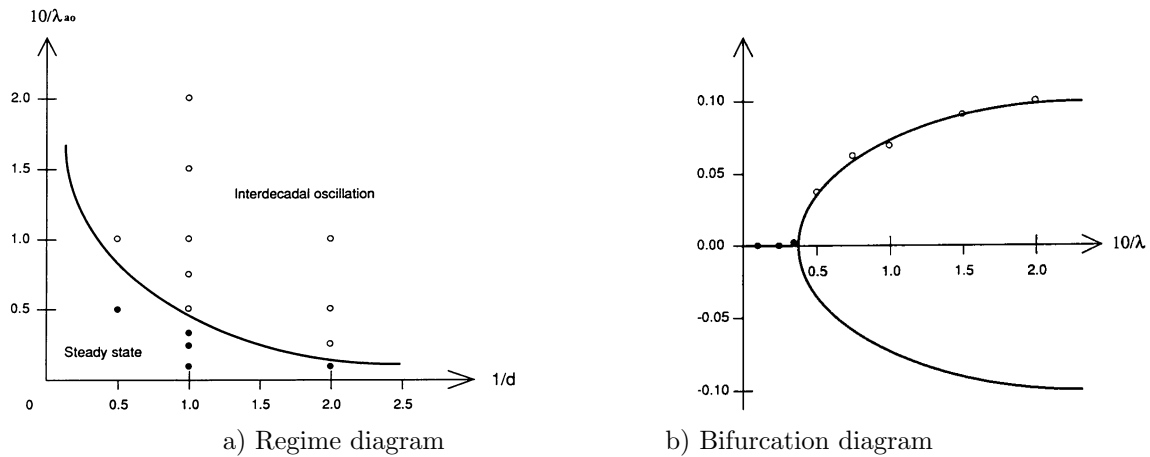


Fig. 1.3. Dependence of THC solutions on two parameters in a hybrid coupled model; the two parameters are the atmosphere-ocean coupling coefficient  $\lambda_{ao}$  and the atmospheric thermal diffusion coefficient  $d$ . (a) Schematic regime diagram. The full circles stand for the models stable steady states, the open circles for stable limit cycles, and the solid curve is the estimated neutral stability curve between the former and the latter. (b) Hopf bifurcation curve at fixed  $d = 1.0$  and varying  $\lambda_{ao}$ ; this curve was obtained by fitting a parabola to the models numerical-simulation results, shown as full and open circles. [From Chen and Ghil (1996) with permission from the American Meteorological Society.]

ture with each other in the oceans upper layers. Their centers follow each other anti-clockwise through the northwestern quadrant of the models rectangular domain. Both the period and the spatio-temporal characteristics of the oscillation are thus rather similar to those seen in a fully coupled GCM with realistic geometry. The transition from a stable equilibrium to a stable limit cycle, via Hopf bifurcation, in this hybrid coupled model, is shown in Fig. 1.3(b).

#### 1.4. Randomness and Nonlinearity

##### 1.4.1. What to expect

The geometric (Arnol'd, 1983; Guckenheimer and Holmes, 1983) and the er-

godic (Eckmann and Ruelle, 1985) theory of *deterministic* dynamical systems represent significant achievements of the 20th century. The foundations of the *stochastic* calculus in its second half (Doob, 1953) also led to the birth of a rigorous theory of time-dependent random phenomena. Historically, theoretical developments in climate dynamics have been largely motivated by these two complementary approaches, based on the work of E. N. Lorenz and that of K. Hasselmann [e.g., Lorenz (1963); Hasselmann (1976)], respectively.

It now seems clear that these two approaches complement, rather than exclude each other. Incomplete knowledge of small-, subgrid-scale

processes, as well as computational limitations will always require one to account for these processes in a stochastic way. As a result of sensitive dependence on initial data and on parameters, numerical weather forecasts, as well as climate projections are both expressed these days in probabilistic terms. In addition to the intrinsic challenge of addressing the nonlinearity along with the stochasticity of climatic processes, it is thus more convenient — and becoming more and more necessary — to rely on a model's (or set of models') *probability density function* (PDF) rather than on its individual, point-wise simulations or predictions.

We summarize here results on the surprisingly complex statistical structure that characterizes stochastic nonlinear systems. This complex structure does provide meaningful physical information that is not described by the PDF alone; it lives on a *random attractor*, which extends the concepts of a *strange attractor* and of the *invariant measure* that is supported by it (Ruelle, 2006), from the deterministic to the stochastic framework.

The expository review here follows the literature of random dynamical systems, as covered for instance by Arnold (1998). Our approach emphasizes the pathwise behavior of the system for individual realizations of the noise over the more usual approach of restricting oneself to the properties of the system's PDF when averaged over a hypothetical ensemble of realizations. This approach might be less familiar even for mathematically sophisticated, but non-specialist readers. For a more complete presentation of this pathwise approach, intended for climate dynamists as well as for other non-specialists, we refer to Ghil *et al.* (2008a) and Chekroun *et al.* (2011b).

#### 1.4.2. *What one finds*

On the road to including random effects, one needs to realize first that the climate system —

as well as any of its subsystems, and on any time scale — is not closed: it exchanges energy, mass and momentum with its surroundings, whether other subsystems or the interplanetary space and the solid earth. The typical applications of dynamical systems theory to climate variability so far have only taken into account exchanges that are constant in time, thus keeping the model — whether governed by ordinary, partial or other differential equations — *autonomous*; i.e., the models had coefficients and forcings that were constant in time.

Succinctly, one can write such a system as

$$\dot{\mathbf{X}} = \mathbf{f}(\mathbf{X}; \boldsymbol{\mu}), \quad (1.7)$$

where  $\mathbf{X}$  now may stand for any state vector or climate field, while  $\mathbf{f}$  is a smooth function of  $\mathbf{X}$  and of the vector of parameters  $\boldsymbol{\mu}$ , but does not depend explicitly on time. This characteristic of being autonomous greatly facilitated the analysis of model solutions' properties. For instance, two distinct trajectories,  $\mathbf{X}_1(t)$  and  $\mathbf{X}_2(t)$ , of a well-behaved, smooth autonomous system cannot pass through the same point in phase space, which helps describe the systems phase portrait. So does the fact that we only need to consider the behavior of solutions  $\mathbf{X}(t)$  as we let time  $t$  tend to  $+\infty$ : the resulting sets of points are — possibly multiple — equilibria, periodic solutions, and chaotic sets. In the language of dynamical systems theory, these are called, respectively: *fixed points*, *limit cycles*, and *strange attractors*.

We know only too well, however, that the seasonal cycle plays a key role in climate variability on many time scales, while orbital forcing is crucial on the Quaternary time scales of many millennia, and now anthropogenic forcing is of utmost importance on interdecadal time scales. How can one take into account such time-dependent forcings, and analyze the non-autonomous systems, written succinctly as

$$\dot{\mathbf{X}} = \mathbf{f}(\mathbf{X}, t; \boldsymbol{\mu}), \quad (1.8)$$

to which they give rise? In Eq. (1.8), the dependence of  $\mathbf{f}$  on  $t$  may be periodic,  $\mathbf{f}(\mathbf{X}, t + P) =$

$\mathbf{f}(\mathbf{X}, t)$ , as in various El Niño–Southern Oscillation (ENSO) models, where the period  $P = 12$  months, or monotone,  $\mathbf{f}(\mathbf{X}, t + \tau) \geq \mathbf{f}(\mathbf{X}, t)$  for  $\tau \geq 0$ , as in studying scenarios of anthropogenic climate forcing.

To illustrate the fundamental character of the distinction between an autonomous system like (1.7) and a non-autonomous one like (1.8), consider the simple scalar version of these two equations:

$$\dot{X} = -\beta X, \tag{1.9}$$

and

$$\dot{X} = -\beta X + \gamma t, \tag{1.10}$$

respectively. We assume that both systems are dissipative, i.e.  $\beta > 0$ , and that the forcing is monotone increasing,  $\gamma \geq 0$ , as would be the case for anthropogenic forcing in the industrial era. Lorenz (1963) pointed out the key role of dissipativity in giving rise to strange, but attracting solution behavior, while Ghil and Childress (1987) emphasized its importance and pervasive character in climate dynamics. Clearly the only attractor for the solutions of Eq. (1.9), given any initial point  $X(0) = X_0$ , is the fixed point  $X = 0$ , attained as  $t \rightarrow +\infty$ .

For the non-autonomous case of Eq. (1.10), though, this *forward-in-time approach* yields blow-up as  $t \rightarrow +\infty$ , for any initial point. To make sense of what happens in the case of time-dependent forcing, one introduces instead the *pullback approach*, in which solutions are allowed to still depend on the time  $t$  at which we observe them, but also on a time  $s$  from which the solution is started,  $X(s) = X_0$ ; presumably  $s \ll t$ . With this little change of approach, one can easily verify that

$$|X(s, t; X_0) - \mathcal{A}(t)| \rightarrow 0 \quad \text{as } s \rightarrow -\infty, \tag{1.11}$$

for all  $t$  and  $X_0$ , where

$$\mathcal{A}(t) = \frac{\gamma(t - 1/\beta)}{\beta}. \tag{1.12}$$

We thus obtain, in this pullback sense, the intuitively obvious result that the solutions, if

started far enough in the past, all approach the attractor set  $\mathcal{A}(\omega)$ , which has a linear growth in time and thus follows the linear forcing.

Let us return now to the more general, non-linear case of Eq. (1.8) and add not only deterministic time dependence  $\mathbf{f}(\mathbf{X}, t)$ , but also random forcing (Ledrappier and Young, 1988; Arnold, 1998),

$$d\mathbf{X} = \mathbf{f}(\mathbf{X}, t)dt + \mathbf{g}(\mathbf{X})d\eta, \tag{1.13}$$

where  $\eta = \eta(t; \omega)$  represents a Wiener process — and  $d\eta(t)$  is commonly referred to as “white noise” — while  $\omega$  labels the particular realization of this random process. The case  $\mathbf{g}(\mathbf{X}) = \mathbf{const.}$  is the case of additive noise, while in the case of  $\partial\mathbf{g}(\mathbf{X})/\partial\mathbf{X} \neq 0$  we speak of multiplicative noise. The distinction between  $dt$  and  $d\omega$  in Eq. (1.13) is necessary since, roughly speaking and following Einstein’s treatment of Brownian motion (Einstein, 1905), it is the variance of a Wiener process that is proportional to time and thus  $d\eta \sim (dt)^{1/2}$ .

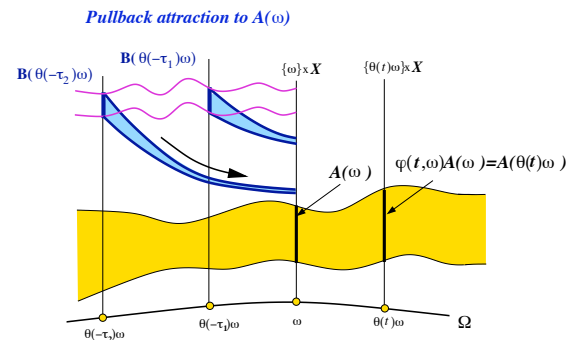


Fig. 1.4. Schematic diagram of a random attractor  $\mathcal{A}(\omega)$  and of the pullback attraction to it; here  $\omega$  labels the particular realization of the random process  $\theta(t)\omega$  that drives the system. We illustrate the evolution in time  $t$  of the random process  $\theta(t)\omega$  (solid black line at the bottom); the random attractor  $\mathcal{A}(\omega)$  itself (yellow band in the middle) with the “snapshots”  $\mathcal{A}(\omega) = \mathcal{A}(t = 0; \omega)$  and  $\mathcal{A}(t; \omega)$  (the two vertical sections, heavy solid); and the flow of an arbitrary set  $\mathcal{B}$  from pullback times  $t = -\tau_2$  and  $t = -\tau_1$  onto the attractor (heavy blue arrows). [After Ghil *et al.* (2008a) with permission from Elsevier.]

In the case of random forcing, we can illus-

trate the concepts introduced by the simple example of Eqs. (1.11, 1.12) above by the random attractor  $\mathcal{A}(\omega)$  (yellow band) of Fig. 1.4. In the figure,  $d\eta(t; \omega) = \theta(t)\omega$  is the random process that drives the system (solid black line) and the pullback attraction is depicted by the flow of an arbitrary set  $\mathcal{B}$  from “pullback times  $t = -\tau_2$  and  $t = -\tau_1$  onto the attractor (heavy blue arrows).

More explicitly, we show in Fig. 1.5 four snapshots  $\{\mathcal{A}_j(\omega) = \mathcal{A}(\omega; t = t_j) : j = 1, 2, 3, 4\}$  that correspond to the vertical cross-sections (heavy solid) in the attractor of Fig. 1.4; a short video, from which these snapshots are taken, appears as Supplementary Information in Chekroun *et al.* (2011b). These snapshots were calculated for the random attractor  $\mathcal{A}(t; \omega)$  of a stochastically perturbed Lorenz system, given by

$$dX = Pr(Y - X)dt + \sigma X d\eta, \quad (1.14a)$$

$$dX = (rX - Y - XZ)dt + \sigma Y d\eta \quad (1.14b)$$

$$dX = (-bZ + XY)dt + \sigma Z d\eta. \quad (1.14c)$$

The parameters  $r$ ,  $Pr$  and  $b$  in Eqs. (1.14) have the usual meanings for 2-D thermal convection:  $r = R/R_c$  is the Rayleigh number  $R$  normalized by its critical value  $R_c$  at the onset of convection,  $Pr$  is the Prandtl number, and  $b$  is a normalized wave number for the most unstable wave at the onset of convection. The noise in this case is multiplicative: its intensity  $\sigma = 0.5$  is multiplied in each one of the three coupled, nonlinear equations above by the corresponding variable  $X, Y$  or  $Z$ .

To be precise, what is plotted in Fig. 1.5, and in the associated video, is the density of the invariant measure  $\nu(\omega)$  supported on the random attractor of the stochastically perturbed Lorenz system governed by Eq. (1.14). In the standard literature of random dynamical systems (Arnold, 1998), these time- and realization-dependent measures are called *disintegrated measures*, since it is their integration with respect to the realizations  $\omega$  over the probability space  $\Omega$  in which they live that yields

— under suitable technical assumptions of existence and uniqueness — the system’s time-invariant PDF. We prefer the more intuitive name of *sample measures*, introduced by the pioneering paper of Ledrappier and Young (1988).

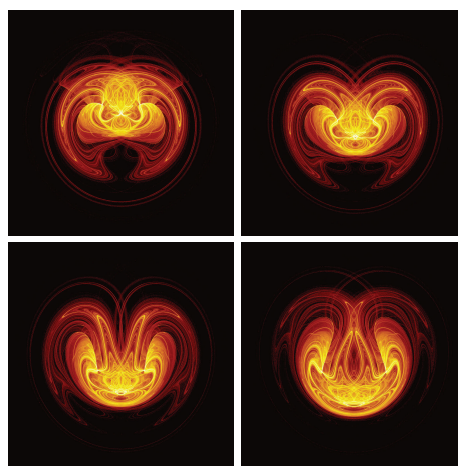


Fig. 1.5. Four snapshots of the stochastically perturbed Lorenz (1963) model’s random attractor  $\mathcal{A}(\omega)$  and the invariant measure  $\nu(\omega)$  supported on it. The parameter values are the classical ones — normalized Rayleigh number  $r = 28$ , Prandtl number  $Pr = 10$ , and normalized wave number  $b = 8/3$  — while the noise intensity is  $\sigma = 0.5$  and the time step is  $\delta t = 5 \cdot 10^3$ . The color bar used is on a log-scale and quantifies the probability to end up in a particular region of phase space; shown is a projection of the 3-D phase space  $(X, Y, Z)$  onto the  $(X, Z)$ -plane. Notice the complex, interlaced filamentary structures between highly (yellow) and moderately (red) populated regions. The time interval  $\Delta t$  between two successive snapshots — moving from left to right and from top to bottom — is  $\Delta t = 0.0875$ . Note that the support of the invariant measure  $\nu(t; \omega)$  may change quite abruptly, from time  $t$  to time  $t + \Delta t$ ; see the related short video in Chekroun *et al.* (2011b). Weakly populated regions cover an important part of the random attractor and are, in turn, entangled with regions that have near-zero probability (black). [After Chekroun *et al.* (2011b) with permission from Elsevier.]

Such a sample measure indicates the probability of trajectories winding up in a particular region of phase space and it is very highly concentrated on the attractor, as inferred from the huge range of density values: the color bar in the figure is on a logarithmic scale, and extends over more than 10 orders of magnitude. The sit-

uation is thus very different from that expected when studying additive noise — in that case, the noise tends to smear out the fine, Cantor-set-like structure of the deterministic, strange attractor and the associated PDF has non-zero-volume support.

It hardly needs saying that additive noise has been studied in climate dynamics much more extensively than the multiplicative sort, for two reasons: (i) it was easier to do so; and (ii) it was suggested by the simple Brownian motion analogy of “weather  $\simeq$  water molecules” and “climate  $\simeq$  pollen particle,” as proposed by Hasselmann (1976). Across the hierarchy of climate models discussed in the previous two sections of this article, however, it is clear that small-and-fast scales of motion do not enter exclusively in an additive manner: they pop up in many, if not all terms of the governing equations, as summarized in Eq. (1.13) above. The insights offered, therefore, by Fig. 1.5 and the video are likely to be of interest across the hierarchy of models, all the way up to and including coupled GCMs and Earth system models.

The sample measure in Fig. 1.5 exhibits amazing complexity, with fine, very intense filamentation: there is no fuzziness whatsoever in its topological structure, which does evoke the Cantor-set foliation of the deterministic attractor. This fine structure strongly suggests that an object of vanishing volume supports this measure, i.e. that the random attractor  $\mathcal{A}(\omega)$  of system (1.13) has — like the strange attractor of the classical, deterministic version, with  $\sigma = 0$  — dimension smaller than 3.

## 1.5. A Rigorous Definition of Climate Sensitivity

### 1.5.1. *Equilibrium climate sensitivity*

The usual view of climate sensitivity — as reflected in the work of the IPCC (Houghton *et al.*, 1991; Solomon *et al.*, 2007) — is that of climate being in equilibrium, in the absence of external perturbations. In the setting of deterministic, autonomous dynamical systems, this view

can be described by the change in the position of a fixed point,  $\mathbf{X}_0 = \mathbf{X}_0(\mu)$ , as a function of a parameter  $\mu$ .

Going back to Fig. 1.1, we can see how the scalar functional  $\bar{T} = \bar{T}\{\mathbf{X}_0(\mu)\}$ , namely the global-mean temperature, varies as a function of the fractional change  $\mu$  of insolation at the top of the atmosphere; here the fixed point  $\mathbf{X}_0 = \mathbf{X}_0(\mu)$  is the equilibrium solution  $T = T(x; \mu)$  of the EBM given by Eq. (1.2). Climate sensitivity for the present climate is thus simply the partial derivative  $\partial\bar{T}/\partial\mu$ , i.e. the tangent of the angle  $\gamma$  between the upper branch of Fig. 1.1 and the abscissa. The sensitivity increases, in general, as we approach the bifurcation point  $(X_0, \mu_0)$  in Eqs. (1.3) or (1.4), and it decreases away from it.

But we have seen in Secs. 1.3 and 1.4 here that internal climate variability can be better described by limit cycles and strange attractors than by fixed points. Moreover, the presence of time-dependent forcing, deterministic as well as stochastic, introduces additional complexities into the proper definition of climate sensitivity.

### 1.5.2. *Defining climate sensitivity in the presence of variability*

We illustrate in Fig. 1.6 the difference between the ways that a change in a parameter can affect a climate model’s behavior in the case of purely periodic solutions vs. the case of equilibrium solutions. One might still think of the former case as the climate of a simpler world, in which ENSO would be purely periodic, rather than irregular. In this case, climate sensitivity can no longer be defined by a single scalar, like  $\partial\bar{T}/\partial\mu$ , but needs at least three scalars: the sensitivity of the mean temperature along with that of the limit cycle’s frequency (or period) and amplitude.

More generally, the setting of non-autonomous and of random dynamical systems, as described in Sec. 1.4, allows one to examine the interaction of internal climate variability with the forcing, whether natural or anthropogenic, and to provide a definition of climate

sensitivity that takes into account the climate systems non-equilibrium behavior and its time-dependent forcing. Such a definition is of the essence in studying systematically the sensitivity of global climate models (GCMs) to the uncertainties in tens of semi-empirical parameters; it will be given here in terms of the response of the appropriate probability densities to changes in the parameters. A comparison with numerical results on parameter dependence for a somewhat simplified GCM (Neelin et al., 2010) goes beyond the scope of this brief overview, and will be given elsewhere.

As an illustration of the more general sensitivity definition that we are proposing, we consider here the case of an infinite-dimensional, but still relatively simple ENSO model. The model is due to Galanti and Tziperman (2000), and its two dependent variables are sea surface temperature  $T$  in the eastern Tropical Pacific and thermocline depth  $h$  there, as a function of time  $t$ :

$$\dot{T} = f(T(t), h(t)), \tag{1.15a}$$

$$h(t) = g(T, h, F)(t, \tau_1, \tau_2), \tag{1.15b}$$

$$F(t) = 1 + \epsilon \cos(\omega t + \phi). \tag{1.15c}$$

In Eqs. (1.15),  $F$  stands for the seasonal forcing, with period  $2\pi/\omega = 12$  months, and all three variables —  $T, h$  and  $F$  — depend on the time  $t$  and the delays  $\tau_1$  and  $\tau_2$ ; these delays characterize the traveling times along the Equator of eastward Kelvin and westward Rossby waves. Several authors have studied such delay-differential models of ENSO; see Dijkstra (2005) for a review and Ghil et al. (2008b) for further mathematical details on this type of models. Note that this Galanti-Tziperman model is non-autonomous, because of the seasonal forcing, but it is still deterministic.

The solutions of Eqs. (1.15) exhibit periodic, quasi-periodic and chaotic behavior, as well as frequency locking to the time-dependent, seasonal cycle. Thus, in principle, an infinite number of scalars are required to define the dependence of these solutions on the parameters  $\tau_1$  and  $\tau_2$ ; these scalars need to include not just the means of temperature  $T$  and depth  $h$ , but also their variance and higher-order moments. We have chosen in Fig. 1.7 to represent this dependence for the zeroth, second and fourth moments of  $h(t)$ ; more precisely the plotted quantities are the mean, standard deviation and fourth root of the kurtosis.

The fourth quantity plotted in Fig. 1.7 is the relative change in Wasserstein distance  $d_W$  from the same reference solution as for the other three quantities. The Wasserstein distance or “earth mover’s distance”  $d_W$  is the distance between

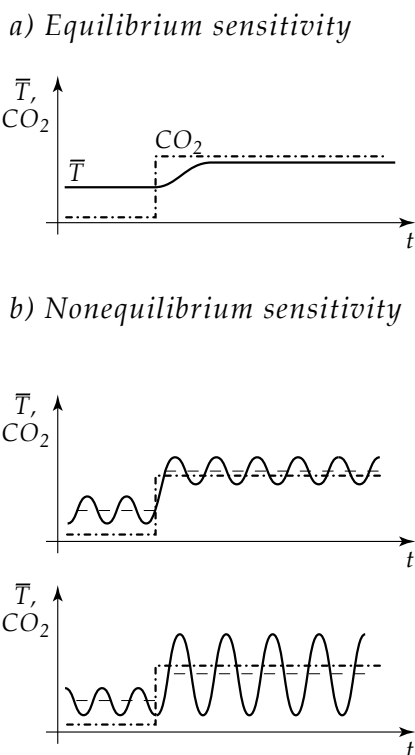


Fig. 1.6. Climate sensitivity (a) for an equilibrium model; and (b) for a nonequilibrium, oscillatory model. As a forcing (atmospheric CO<sub>2</sub> concentration, say, dash-dotted line) changes suddenly, global temperature (heavy solid) undergoes a transition: in panel (a) only the mean temperature changes; in panel (b) the mean (shown now as light dashed) adjusts as it does in panel (a), but the amplitude of the oscillation can also decrease, increase or stay the same.

two measures of equal mass on a metric space, i.e., on a space that has a metric attached to it, like an  $n$ -dimensional Euclidean space (Dobrushin, 1970). Roughly speaking,  $d_W$  represents the total work needed to move the “dirt” (i.e., the measure) from a trench you are digging to another one you are filling, over the distance between the two trenches.

In fact, the mathematician Gaspard Monge — a founder of the Ecole Polytechnique and an officer in Napoleon’s armies — introduced essentially what is now called the Wasserstein distance with precisely this motivation. In general, the shape of the two trenches and the depth along the trench — i.e., the support of the measure and its density — can differ. In the case at hand, the shape and density of the invariant measure that is being moved are plotted in Fig. 1.8.

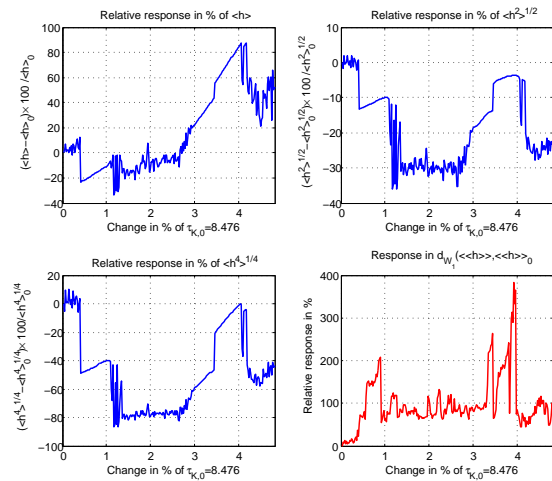


Fig. 1.7. Relative changes in the statistical properties of the thermocline depth  $h(t)$ , for the delay-differential ENSO model of Eq. (1.15) and changes of 05% in the delay parameter  $\tau_K$  associated with the Kelvin wave transit: (a) mean; (b) second moment; (c) fourth moment; and (d) Wasserstein distance  $d_W$ . Note intervals of both smooth and rough dependence of the solution on the parameter. [Courtesy of M.D. Chekroun.]

More recently,  $d_W$  has become hugely popular in many contexts that involve related problems. Hairer and Mattingly (2006) have used

it in proving certain properties of an invariant measure for the Markov semi-group associated with the 2-D Navier-Stokes equations driven by additive noise. Likewise, Hairer and Majda (2010) used it in proving the differentiability of the invariant measure for stochastic differential equations in the presence of a large class of noise processes, i.e. in the so-called hypo-elliptic case. The latter authors also did mention climate dynamics as an interesting area of applications of their work.

It is quite clear from Fig. 1.7 that intervals of smooth dependence of the solution on the parameter alternate with jumps and with intervals of rough dependence. The jump points are the same in all four panels of the figure and there is agreement also in the smooth vs. rough intervals, although the Wasserstein distance in panel (d) shows some roughness even over intervals in which the three statistical moments in panels (a–c) behave smoothly. The latter point is not too surprising, since  $d_W$  contains more information than each of the moments.

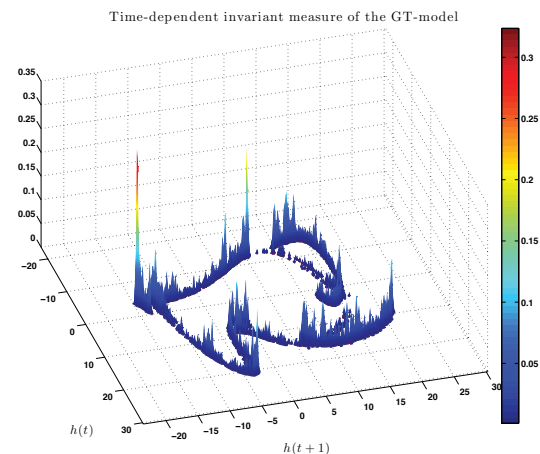


Fig. 1.8. Time-dependent invariant measure of the Galanti and Tziperman (2000) model, plotted in an isometric projection with the probability density on the perpendicular to the plane spanned by the coordinates  $(h(t), h(t + 1))$ . The time here is in units of years, and the density is highly concentrated on a very “thin” support, as for the stochastically perturbed Lorenz model in Fig. 1.5. [Courtesy of M.D. Chekroun.]

The very high concentration of probability density in the peak at the extreme left of Fig. 1.8 might seem surprising but actually agrees with such a peak in the stochastically perturbed ENSO model of Timmermann and Jin (2002). The latter model is based on three ordinary differential equations, for sea surface temperatures in the eastern and western Tropical Pacific and for thermocline depth, and it was analyzed in detail by Chekroun *et al.* (2011b). The corresponding near-singularity in invariant measure on the model's random attractor evolves regularly in time and thus suggests that the interaction of deterministic nonlinearities with time-dependent forcing, including even stochastic perturbations, can help seasonal-to-interannual prediction, rather than hinder it. Chekroun *et al.* (2011a) have taken some interesting steps in exploiting this possibility.

With the results illustrated in Figs. 1.7 and 1.8 in hand, it becomes natural to define climate sensitivity in the presence of internal variability and of time-dependent forcing as the partial derivative of the Wasserstein distance  $d_W$  with respect to a parameter  $\mu$ ,  $\partial d_W / \partial \mu$ . Clearly,  $d_W$  has to be defined in turn with respect to the particular climate whose sensitivity we wish to evaluate.

At this time, it would be awkward, difficult or even impossible to compute with absolute accuracy the function  $d_W = d_W(\mu)$  and its derivative at  $\mu = \mu_0$ ; but reasonable approximations should become available shortly, as is the case already for the calculation of the invariant measures of models of intermediate complexity. We outline a way to proceed in this direction in Sec. 1.6 below.

The definition given here for a deterministic but non-autonomous ENSO model can be generalized further to the random case, assuming the existence of the suitable invariant measures. The advantage of using the definition of climate sensitivity  $\partial d_W / \partial \mu$  proposed herein over the customary one of  $\partial \bar{T} / \partial \mu$  is twofold. First, it makes sense for any climate model with natu-

ral variability and with time-dependent forcing. Second, it involves the sensitivity of the higher-order moments of the model's PDF, up to and including changes in the model's extreme events. Interest in the latter has been increasing dramatically in recent years [e.g., Yiou and Nogaj (2004); Ghil *et al.* (2011)], along with the realization that changes in mean global temperature  $\bar{T}$  are not that interesting in and of themselves.

A complementary approach to climate sensitivity out of equilibrium is the one based on the *fluctuation-dissipation theory (FDT)* of statistical mechanics (Leith, 1975; Ghil *et al.*, 1985; Lucarini and Sarno, 2011; Wouters and Lucarini, 2013). The complementarity arises from D. Ruelle's extending the many-particle, statistical-mechanics ideas to low-order dynamical systems subject to certain mathematical conditions on the latter (Ruelle, 1997, 1999; Chekroun *et al.*, 2011b).

The key concept underlying both approaches is that of *linear response* in a highly nonlinear system. Important results in applying this concept have been obtained across the modeling hierarchy by several authors (Gritsun, 2001; Gritsun and Branstator, 2007; Majda and Wang, 2010).

We thus expect the theory of random dynamical systems, along with FDT, to provide robust tools for studying the parameter dependence of a nonlinear, randomly perturbed system's various "metrics." These metrics — a word used by the climate community in a much broader sense than the standard mathematical term — can include global quantities, like mean temperature or total energy, but also much finer functionals of the state of the system, such as regional temperatures or precipitation. In addition, random dynamical systems theory can help improve prediction of future system properties, by relying on a judicious combination of the history of its slow and fast behavior (Chekroun *et al.*, 2011a).

## 1.6. Concluding Remarks

A complete theory of climate variability and climate sensitivity, across the entire range of time scales of interest, is still in the future. We have shown, though, that powerful conceptual and numerical tools exist in order to organize the emerging knowledge so far. The approach described herein relies on applying systematically dynamical systems theory, both deterministic and stochastic, across a hierarchy of models, from the simplest toy models to the most detailed, coupled GCMs.

The dynamical systems approach has progressed from its first modest steps, taken half-a-century ago, to the analysis of the behavior of atmospheric, oceanic and coupled GCMs over the last two decades. We have reviewed, in particular, the robustness of fundamental bifurcations — namely those associated with multiple equilibria and with transition from equilibrium to oscillatory behavior — across the model hierarchy, for models that treat the Earth system's energy balance and for those that treat the oceans' thermohaline circulation. Particularly interesting strides have been taken over the last decade in studying the interaction of the faster time scales with the slower ones, within a genuinely nonlinear framework.

A number of GCMs — particularly some of those used in numerical weather prediction and in seasonal-to-interannual forecasting — combine a deterministic representation of large-scale processes, in particular of the fluid dynamics, with a stochastic parametrization of one or more of the small-scale physical processes, such as cloud feedbacks (Lin and Neelin, 2003; Palmer and Williams, 2009). Furthermore, the stochastic parametrizations are often of the multiplicative-noise type discussed herein.

Typically — as discussed by Neelin *et al.* (2010), among others — the GCM team in question will verify that a particular stochastic parametrization does achieve a particular improvement aimed at in developing it. But it

has been difficult so far to check how one or another such parametrization does affect the GCM's overall performance, in particular its sensitivity to changes in certain parameter values or in other parametrizations. The concepts and tools reviewed herein should help in carrying out more systematically such climate model sensitivity studies.

How to do so in practice raises, of course, the question of how to approximate in a useful way the pullback attractor of a GCM or of high-dimensional models in general? First of all, we remind the reader that the Galanti and Tziperman (2000) model studied in Sec. 1.5.2 here is an infinite-dimensional model; it falls short of the complexity of a GCM but its evolution in time still needed to be computed by suitable numerical approximations.

More generally, the empirical model reduction (EMR) approach (Kondrashov *et al.*, 2005; Kravtsov *et al.*, 2005, 2009) provides precisely the required kind of reduction from a high-dimensional model, like a GCM, to a low-order model that is both nonlinear and noise-driven. EMR models based on this approach have proven to be particularly skillful at capturing and simulating the power spectrum of higher-order models, as well as their PDF in the phase space of the leading empirical orthogonal functions (Kravtsov *et al.*, 2005). Barnston *et al.* (2012) have shown that real-time ENSO prediction by an EMR model (Kondrashov *et al.*, 2005) is highly competitive among two dozen dynamical and statistical forecasts in the ENSO multi-model prediction plume of the International Research Institute for Climate and Society at Columbia University.

The obvious route to studying the pullback attractor of a GCM is to first approximate the GCM by an EMR model, using a sufficiently long simulation or ensemble of simulations of the GCM. The next step is to study the pullback attractor of the EMR, in the same way as done in Secs. 1.4.2 and 1.5.2 here.

Doing so should include a study of the EMR model's sensitivity, as defined herein, to cover changes in its variability, including extreme events, as well as in its mean. This is not to say that such a study will be easy or give the right answers right away. But it should provide an interesting start in the right direction.

### Acknowledgments

It is a pleasure to thank Mickael D. Chekroun for Figs. 1.7 and 1.8. Discussions with him and with several other colleagues — including but not restricted to D. Kondrashov, J. C. McWilliams, J. D. Neelin, E. Simonnet, S. Wang, and I. Zaliapin — have helped develop the ideas in this chapter, and more particularly those formulated in Sec. 1.5. Equation (1.6) and the associated discussion in Sec. 1.3.2 is based on a talk given by Henk A. Dijkstra at a meeting on “Mathematical Paradigms of Climate Science” in Rome, June 2013. Thoughtful and constructive comments by two anonymous reviewers have helped improve the presentation. Related work is partially supported by NSF grant DMS-0934426 and by by ONR-MURI grant N00014-12-1-0911.

### References

- Andronov, A. A., and L. S. Pontryagin, 1937: Systèmes grossiers. *Dokl. Akad. Nauk SSSR*, **14**(5), 247–250.
- Arnold, L., 1998: *Random Dynamical Systems*. Springer-Verlag, New York/Berlin, 602 pp.
- Arnol'd, V. I., 1983: *Geometric Methods in the Theory of Ordinary Differential Equations*. Springer-Verlag, New York/Berlin, 334 pp.
- Barnston, A. G., M. K. Tippett, M. L. Heurreux, S. Li, and D. G. DeWitt, 2012: Skill of real-time seasonal ENSO model predictions during 2002–2011 — is our capability improving?, *Bull. Am. Meteorol. Soc.*, **93**, 631–651.
- Bryan, F., 1986: High-latitude salinity effects and interhemispheric thermohaline circulations. *Nature*, **323**, 301–304.
- Bryden, H. L., B. A. King, and G. D. McCarthy, 2011: South Atlantic overturning circulation at 24 S. *J. Mar. Res.*, **69**, 38–55, doi:10.1357/002224011798147633.
- Budyko, M. I., 1969: The effect of solar radiation variations on the climate of the Earth. *Tellus*, **21**, 611–619.
- Charney, J. G., A. Arakawa, D. J. Baker, et al., 1979: *Carbon Dioxide and Climate: A Scientific Assessment*. National Academies Press, Washington, D.C., 34 pp.
- Chekroun, M. D., D. Kondrashov, and M. Ghil, 2011a: Predicting stochastic systems by noise sampling, and application to the El Niño–Southern Oscillation. *Proc. Natl. Acad. Sci. USA*, **108**(29), 11,7660–11,771, doi:10.1073/pnas.1015753108.
- , E. Simonnet, and —, 2011b: Stochastic climate dynamics: Random attractors and time-dependent invariant measures. *Physica D*, **240**(21), 1685–1700, doi:10.1016/j.physd.2011.06.005.
- Chen, F., and M. Ghil, 1996: Interdecadal variability in a hybrid coupled ocean-atmosphere model. *J. Phys. Oceanogr.*, **26**, 1561–1578.
- Dijkstra, H. A., 2005: *Nonlinear Physical Oceanography: A Dynamical Systems Approach to the Large-Scale Ocean Circulation and El Niño*, 2nd ed., Kluwer Acad. Publishers, Dordrecht/Norwell, Mass., 532 pp.
- , 2007: Characterization of the multiple equilibria regime in a global ocean model. *Tellus*, **59A**, 695–705.
- , and M. Ghil, 2005: Low-frequency variability of the large-scale ocean circulation: A dynamical systems approach. *Rev. Geophys.*, **43**, RG3002, doi:10.1029/2002RG000122.
- Dobrushin, R. L., 1970: Prescribing a system of random variables by conditional distributions. *Theor. Prob. Appl.*, **15**, 458–486.
- Doob, J. L., 1953: *Stochastic Processes*. Wiley, New York, 654 pp.
- Drijfhout, S., S. Weber, and E. van der Swaluw, 2011: The stability of the MOC as diagnosed from model projections for pre-industrial, present and future climates. *Clim. Dyn.*, **37**, 1575–1586, doi:10.1007/s00382-010-0930-z.
- Eckmann, J.-P., and D. Ruelle, 1985: Ergodic theory of chaos and strange attractors. *Rev. Mod. Phys.*, **57**, 617–656 (addendum, *Rev. Mod. Phys.*, **57**, 1115).
- Einstein, A., 1905: On the movement of small particles suspended in a stationary liquid demanded by the molecular-kinetic theory of

- heat, *Ann. d. Physik (Leipzig)*, **17**, 549 ff., reprinted in *Investigations on the Theory of the Brownian Movement, five articles by A. Einstein*, Fürth, R. (Ed.) and A. D. Cowper (transl.) (1956, Dover Publ., New York), 122 pp.
- Galanti, E., and E. Tziperman, 2000: ENSO's phase locking to the seasonal cycle in the fast-SST, fast-wave, and mixed-mode regimes. *J. Atmos. Sci.*, **57**, 2936–2950.
- Ghil, M., 1976: Climate stability for a Sellers-type model. *J. Atmos. Sci.*, **33**, 3–20.
- , 1994: Cryothermodynamics: The chaotic dynamics of paleoclimate. *Physica D*, **77**, 130–159.
- , 2001: Hilbert problems for the geosciences in the 21st century. *Nonlin. Processes Geophys.*, **8**, 211–222.
- , R. Benzi, and G. Parisi, Ed., 1985: *Turbulence and Predictability in Geophysical Fluid Dynamics and Climate Dynamics*. North-Holland, Amsterdam, 449 pp.
- , and S. Childress, 1987: *Topics in Geophysical Fluid Dynamics: Atmospheric Dynamics, Dynamo Theory and Climate Dynamics*. Springer-Verlag, New York/Berlin, 485 pp.
- , and A. W. Robertson, 2000: Solving problems with GCMs: General circulation models and their role in the climate modeling hierarchy. *General Circulation Model Development: Past, Present and Future*, D. Randall, Ed., Academic Press, San Diego, pp. 285–325.
- , A. Mullhaupt, and P. Pestiaux, 1987: Deep water formation and Quaternary glaciations. *Climate Dyn.*, **2**, 1–10.
- , M. R. Allen, M. D. Dettinger, et al., 2002: Advanced spectral methods for climatic time series. *Rev. Geophys.*, **40**(1), pp. 3.1–3.41, doi: 10.1029/2000RG000092.
- , M. D. Chekroun, and E. Simonnet, 2008a: Climate dynamics and fluid mechanics: Natural variability and related uncertainties. *Physica D*, **237**, 2111–2126, doi:10.1016/j.physd.2008.03.036.
- , I. Zaliapin, and S. Thompson, 2008b: A delay differential model of ENSO variability: parametric instability and the distribution of extremes. *Nonlin. Processes Geophys.*, **15**, 417–433.
- , P. Yiou, S. Hallegatte, et al., 2011: Extreme events: Dynamics, statistics and prediction. *Nonlin. Processes Geophys.*, **18**, 295–350, doi:10.5194/npg-18-295-2011.
- Gritsun, A. S., 2001: Fluctuation-dissipation theorem on attractors of atmospheric models. *Russ. J. Numer. Analysis Math. Modell.*, **16**, 97–190.
- Gritsun, A. S., and G. Branstator, 2011: Climate response using a three-dimensional operator based on the fluctuation dissipation theorem. *J. Atmos. Sci.*, **64**, 2558–2575.
- Guckenheimer, J., and P. Holmes, 1983: *Nonlinear Oscillations, Dynamical Systems and Bifurcations of Vector Fields*. Springer-Verlag, New York/Berlin, 453 pp.
- Hairer, M., and J. C. Mattingly, 2006: Ergodicity of the 2D Navier-Stokes equations with degenerate stochastic forcing. *Annals Math.*, **164**, 993–1032.
- Hairer, M., and A. J. Majda, 2010: A simple framework to justify linear response theory. *Nonlinearity*, **23**, 909–922.
- Hasselmann, K., 1976: Stochastic climate models, Part I: Theory. *Tellus*, **28**, 473–485.
- Hawkins, E., R. S. Smith, L. C. Allison, J. M. Gregory, T. J. Woollings, H. Pohlmann, and B. de Cuevas, 2011: Bistability of the Atlantic overturning circulation in a global climate model and links to ocean freshwater transport. *Geophys. Res. Lett.*, **38**, doi:10.1029/2011GL047208.
- Held, I. M., and M. J. Suarez, 1974: Simple albedo feedback models of the ice caps. *Tellus*, **26**, 613–629.
- Houghton, J. T., G. J. Jenkins, and J. J. Ephraums, Ed., 1991: *Climate Change, The IPCC Scientific Assessment*. Cambridge Univ. Press, Cambridge, MA, 365 pp.
- Kalnay, E., 2003: *Atmospheric Modeling, Data Assimilation and Predictability*. Cambridge Univ. Press, Cambridge/London, UK, 341 pp.
- Kennett, R. P., and L. D. Stott, 1991: Abrupt deep-sea warming, paleoceanographic changes and benthic extinctions at the end of the Palaeocene. *Nature*, **353**, 225–229.
- Kondrashov, D., S. Kravtsov, A. W. Robertson, and M. Ghil, 2005: A hierarchy of data-based ENSO models. *J. Climate*, **18**, 4425–4444.
- Kravtsov, S., D. Kondrashov, and M. Ghil, 2005: Multilevel regression modeling of nonlinear processes: Derivation and applications to climatic variability. *J. Climate*, **18**, 4404–4424.
- Kravtsov, S., D. Kondrashov, and M. Ghil, 2009: Empirical model reduction and the modeling hierarchy in climate dynamics, in *Stochastic Physics and Climate Modeling*, edited by T. N.

- Palmer and P. Williams, pp. 35–72, Cambridge Univ. Press.
- Ledrappier, F., and L.-S. Young, 1988: Entropy formula for random transformations. *Prob. Theory Related Fields*, **80**, 217–240.
- Leith, C. E., 1975: Climate response and fluctuation dissipation. *J. Atmos. Sci.*, **32**, 2022–2026.
- Li, Z.-X., K. Ide, H. Le Treut, et al., 1997: Atmospheric radiative equilibria in a simple column model. *Clim. Dyn.*, **13**, 429–440.
- Lin, J. W. B., and J. D. Neelin, 2003: Toward stochastic deep convective parameterization in general circulation models. *Geophys. Res. Lett.*, **30**, 1162, doi:10.1029/2002GL016203.
- Lorenz, E. N., 1963: Deterministic nonperiodic flow. *J. Atmos. Sci.*, **20**, 130–141.
- Lucarini, V., and S. Sarno, 2011: A statistical mechanical approach for the computation of the climatic response to general forcings. *Nonlin. Processes Geophys.*, **18**, 7–28, doi:10.5194/npg-18-7-2011.
- Majda, A. J., and X. Wang, 2010: Linear response theory for statistical ensembles in complex systems with time-periodic forcing. *Commun. Math. Sci.*, **8**, 145172.
- Marotzke, J., 2000: Abrupt climate change and thermohaline circulation: Mechanisms and predictability. *Proc. Natl. Acad. Sci. USA*, **97**, 1347–1350.
- Neelin, J. D., A. Bracco, H. Luo, et al., 2010: Considerations for parameter optimization and sensitivity in climate models. *Proc. Natl. Acad. Sci. USA*, **107**(50), 21,349–21,354.
- North, G. R., 1975: Analytical solution to a simple climate model with diffusive heat transport. *J. Atmos. Sci.*, **32**, 1301–1307.
- , J. G. Mengel and D. A. Short, 1983: Simple energy-balance model resolving the seasons and the continents - application to the astronomical theory of the ice ages. *J. Geophys. Res.*, **88**, 6576–6586.
- Palmer, T. N., and P. Williams (Eds.), 2009: *Stochastic Physics and Climate Modelling*. Cambridge University Press.
- Ramanathan, V., and J. A. Coakley, 1978: Climate modeling through radiative convective models. *Rev. Geophys. Space Phys.*, **16**, 465–489.
- Ruelle, D., 1997: Application of hyperbolic dynamics to physics: Some problems and conjectures. *Bull. Amer. Math. Soc.*, **41**, 275–278.
- Ruelle, D., 2009: A review of linear response theory for general differentiable dynamical systems. *Nonlinearity*, **22**, 855–870.
- Ruelle, D., 2006: What is a strange attractor? *Notices Amer. Math. Soc.*, **53**, 764–765.
- , and F. Takens, 1971: On the nature of turbulence. *Commun. Math. Phys.*, **20**, 167–192, and **23**, 343–344.
- Schneider, S. H., and R. E. Dickinson, 1974: Climate modeling. *Rev. Geophys. Space Phys.*, **25**, 447–493.
- Sellers, W. D., 1969: A global climatic model based on the energy balance of the earth-atmosphere system. *J. Appl. Meteor.*, **8**, 392–400.
- Solomon, S., D. Qin, M. Manning, et al., Eds., 2007: *Climate Change 2007: The Physical Science Basis. Contribution of Working Group I to the Fourth Assessment Report of the IPCC*. Cambridge Univ. Press, Cambridge/London, UK, 996 pp.
- Stommel, H., H., 1961: Thermohaline convection with two stable regimes of flow. *Tellus*, **13**, 224–230.
- Timmermann, A., and F.-F. Jin, 2002: A nonlinear mechanism for decadal El Niño amplitude changes. *Geophys. Res. Lett.*, **29** (1), 1003, doi:10.1029/2001GL013369.
- Wetherald, R. T., and S. Manabe, 1975: The effect of changing the solar constant on the climate of a general circulation model. *J. Atmos. Sci.*, **32**, 2044–2059.
- Wouters, J., and V. Lucarini, 2013: Parametrization of cross-scale interaction in multi-scale systems. (*In this volume, pp. yyy–zzz.*)
- Yiou, P., and N. Nogaj, 2004: Climatic extremes and weather regimes: Where and when? *Geophys. Res. Lett.*, **31**, L07202 10.1029/2003GL019119.